Environmental Microbiology, **17**, 4600–4614

Involvement of a caleosin in lipid storage, spore dispersal, and virulence in the entomopathogenic filamentous fungus, *Beauveria bassiana*

Yanhua Fan,[1,2] Almudena Ortiz-Urquiza,[2] Timothy Garrett,[3] Yan Pei[1] and Nemat O. Keyhani[2]*

[1]*Biotechnology Research Center, Southwest University, Chongqing, Beibei, China.*

[2]*Department of Microbiology and Cell Science, Institute of Food and Agricultural Sciences, University of Florida, Gainesville, FL 32611, USA.*

[3]*Department of Pathology, Immunology, and Laboratory Medicine, College of Medicine, University of Florida, Gainesville, FL 32610, USA.*

Summary

Eukaryotic cells store lipids in membrane-encased droplets. The entomopathogenic fungus, *Beauveria bassiana*, initiates infection via attachment of its spores to the epicuticle or waxy layer of target insects, degrading and assimilating host surface hydrocarbons, carbohydrates and proteins. Caleosins are components of the proteinaceous coat of lipid droplets and a single *B. bassiana* caleosin homologue, *Bbcal1*, was identified and characterized. The BbCal1 sequence contained an EF-hand Ca^{2+} binding domain and potential hydrophobic stretches similar to those found in plant caleosins, along with a proline knot motif defined by only two proline resi-dues. Targeted gene inactivation of *Bbcal1* did not appear to affect spore germination, growth on lipid substrates or stress response, but changes in lipid, vacuole and endoplasmic reticulum/multilamellar vesicle-like structures and altered cellular lipid pro-files were seen in conidia grown on a variety of sub-strates including potato dextrose agar, olive oil, glyceride trioleate, oleic acid and the alkane, C16. The*Bbcal1* mutant produced more compact assem-blages of conidia, displayed a reduced and delayed spore dispersal phenotype, and showed decreased virulence in insect bioassays using the greater wax moth, *Galleria mellonella*. Our data indicate novel functions for caleosins in fungal virulence, spore development and the trafficking and/or turnover of lipid-related structures.

Introduction

The canonical structures for lipid storage in eukaryotic cells are lipid droplets (LDs), whose major components are neutral lipids, e.g. triacylglycerols and sterol esters, the latter mainly cholesterol in animals and ergosterol in fungi, encased in a phospholipid monolayer (Pol *et al*., 2014). LDs bud from the endoplasmic reticulum (ER) where the neutral lipids are synthesized and sequestered into a surrounding amphipathic lipid layer interspersed with various protein constituents. Misregulation of LD for-mation and/or turnover has been implicated in a wide variety of human diseases including diabetes and obesity, as well as liver, cardiac and muscle pathologies (Greenberg *et al*., 2011). In mammals and fungi, the mem-brane monolayers of LDs chiefly consist of phosphatidyls -choline (50–60%) and -ethanolamine (20–30%), embed-ded with proteins that include the perilipins found in mammals, arthropods and fungi (Sztalryd and Kimmel, 2014). Perilipins regulate LD formation via control of lipolysis by recruiting or preventing lipase access to the LD (Bickel *et al*., 2009). In fungi, perilipins appear to be restricted to the Pezizomycotina, which represents the largest subphylum of the Ascomycota and includes many plant, animal and arthropod pathogens, but excludes the Saccharomycotina yeasts, the latter of which do not appear to have perilipin homologues. To date only a single fungal perilipin has been genetically characterized, namely the *MPL1* perilipin of the entomopathogenic fungus *Metarhizium anisopliae* which has been shown to regulate lipid metabolism, formation of infectious struc-tures including the appressorial turgor pressure needed to help breach the insect cuticle and virulence (Wang and Leger, 2007). Caleosins, however, are distinct from the perilipins and the two do not share any appreciable sequence homology.

In plants, LDs have been mainly examined within seed tissues where they serve as energy and carbon resources needed for germination and subsequent early growth, although roles for LDs in other plant tissues, including leaves, flowers, pollen and fruits, are emerging (Frandsen *et al*., 2001; Zienkiewicz *et al*., 2011; Chapman *et al*., 2012; Umate, 2012). Three major plant-LD associated proteins, oleosins, steroleosins (sterol dehydrogenases) and caleosins have been characterized. None of these

proteins possess N-terminal cleavable signal sequences found on most seed storage ER-targeted proteins; instead, all three of these protein families contain a hydro-phobic central region flanked by variable length and amino acid sequence hydrophilic/amphipathic domains. Within the hydrophobic domain (~30–75 amino acids in length), there is a highly conserved set of prolines distrib-uted over a 12- to 15-residue region that forms an antiparallel helix or β-strand, termed a 'proline knot/knob'. The proline knot is required for oil body targeting and extends into the LD in a hairpin-like structure, resulting in both N- and C-terminal domains on the outside of the droplet facing the cytoplasm (Abell *et al*., 1997). In addition to the proline knot motif, oleosins have N-and C-terminal phospholipid binding domains, and steroleosins have hydroxysteroid dehydrogenase domains, typically at the C-terminus (Chapman *et al*., 2012). Caleosins contain an N-terminal helix–loop–helix EF-hand calcium-binding motif, followed by the proline knot, and a subsequent hydrophilic C-terminal domain that contains conserved protein phosphorylation sites (Chen *et al*., 1999). Depending upon the species, caleosins can be major or minor components of plant LDs, where they are thought to act in LD structural mainte-nance and turnover, contributing to various physiological processes including seed germination, and whole plant responses to drought, salt and osmotic stresses (Partridge and Murphy, 2009; Aubert *et al*., 2010; Chapman *et al*., 2012; Umate, 2012). Caleosins or caleosin-like proteins have been identified in LDs isolated from microalgae (*Chlorella* sp.), and more recently from the reef-building coral endosymbiont, *Symbiodinium* spp., where in the latter case LDs have been implicated in contributing to the mutualistic endosymbiosis between the two organisms (Lin *et al*., 2012; Pasaribu *et al*., 2014). Genes encoding for orthologues of caleosins have also been found in fungi including members of the Ascomycete and Basidiomycete phyla; however, the functions of caleosins in fungi have yet to be examined.

Beauveria bassiana, a filamentous Ascomycete insect pathogen, best known as an ecologically friendly alterna-tive to chemical pesticides, is an Environmental Protec-tion Agency-approved insect biological control agent that has been exploited for use against agricultural pests and for insects that act as human and animal disease vectors such as mosquitoes and ticks (Kirkland *et al*., 2004; Fan *et al*., 2012b; Glare *et al*., 2012). A facultative pathogen of arthropods, *B. bassiana* and their insect hosts

represent a model system with which to examine unique and evolutionarily important host–pathogen interactions (He *et al*., 2014; Ortiz-Urquiza and Keyhani, 2015). Infection of insects is percutaneous, with no specialized route of entry required; fungal spores or conidia attach to the cuticles of target hosts and in response to surface cues, the conidia germinate, and the emerging germ tubes produce a variety of enzymes that when combined with mechani-cal pressure begins the process of cuticle penetration (Ortiz-Urquiza and Keyhani, 2013). Once the cuticle has been penetrated, the growing fungal hyphae reach the insect haemocoel, elaborating single yeast-like cells termed hyphal bodies that proliferate on the nutrients present in the haemolymph (Lewis *et al*., 2009; Wanchoo *et al*., 2009). As these nutrients are depleted, the fungus works its way back out of the host body, where it sporulates/conidiates on the insect cadaver. The resultant conidia are the dispersive structures and can grow either saprophytically or infect another host. Conidial attach-ment and interaction to the insect waxy layer (epicuticle), the outermost layer of the cuticle, is the first step in patho-genesis (Holder and Keyhani, 2005; Zhang *et al*., 2011), and *B. bassiana* has evolved the ability to assimilate various insect hydrocarbons and lipids (Pedrini *et al*., 2010; 2013; Zhang *et al*., 2012; Ortiz-Urquiza and Keyhani, 2013). Little, however, is known concerning the molecular aspects of lipid assimilation and/or storage in entomopathogenic fungi. Growth on lipid substrates has been linked to fungal virulence, and *B. bassiana* can grow in hydrocarbon substrates as high as C31–33, with robust growth seen on C16 (Pedrini *et al*., 2010). Here we report on the identification and characterization of a caleosin homologue, *Bbcal1*, in *B. bassiana*. Targeted gene inac-tivation of *Bbcal1* did not result in significant phenotypes with respect to growth on various media including lipids or in under the stress conditions examined. Significant alterations in lipid profiles including phospholipid and ergosterol content were seen and the accumulation of aberrant intracellular structures including multilamellar ER-like bodies was observed under various growth con-ditions. Although overall conidial yield was unaffected, the *Bbcal1* strain produced more compact assemblages of conidia that showed a decreased ability to disperse. In addition, the *Bbcal1* strain showed reduced virulence in insect bioassays using the greater wax moth, *Galleria mellonella*, as the host.

Results

Sequence analysis and generation of Bbcal1 *disruption mutant and gene complementation strains*

A sequence fragment displaying high similarity to caleosins was identified in previously described *B. bassiana* expressed sequence tag libraries (Cho *et al*., 2006a,b). The full-length genomic sequence including 5′ and 3′ flanking sequences was obtained from the *B. bassiana* genome. Analysis of the genomic sequence of *Bbcal1* indicated a 1089 bp long gene with four putative introns (64, 93, 66 and 101 bp, respectively) and encod-ing for a protein of 254 amino acids (mol. wt. = 29 kDa, pI = 6.0). The predicted protein was highly homologous to and shared common features with caleosins, including a C-terminal EF-hand motif, a central hydrophobic proline knot and an N-terminus hydrophilic motif (Fig. S1A). NCBI BLAST and phylogenetic analyses of the *Bbcal1* gene revealed the best homology matches to proteins in the database to be from the entomopathogenic fungus *Cordyceps militaris*, the rice blast fungus *Magnaporthe oryzae*, and the plant cereal pathogen *Colletotrichum graminicola*. Unlike plant caleosins that contain multiple proline residues defining the same region, alignment of the fungal sequences indicated the presence of only two prolines in the 'proline knot' motif (Fig. S1B). In addition, the *C. militaris*, although overall showing the highest simi-larity to the *B. bassiana* sequence, contained an almost 100 amino acid extension at its C-terminus.

A 2.1 kb sequence that included the *Bbcal1* gene and upstream (LB) and downstream (RB) flanking sequences and the *bar* selective marker that confers resistance to phosphinothricin was used to construct the targeted gene knockout vector (Fig. 1A). Approximately 120 transformants were initially screened for the correct inte-gration event by polymerase chain reaction (PCR), of which three appeared to represent targeted disruptions of *Bbcal1*, with the rest representing ectopic integration events (Fig. 1B). Targeted gene disruption mutants were then verified by Southern blotting (Fig. 1C). In addition, reverse transcription-PCR experiments using primers designed to the *Bbcal1* cDNA sequence showed complete loss of the transcripts of the genes in each respective mutant (Fig. 1D). Complementation vectors were con-structed using a 3.1 kb genomic region corresponding to *Bbcal1*. Complemented strains were indistinguishable from the wild-type strain in all phenotypic aspects examined except as noted below.

Loss of Bbcal1 *results in decreased spore dispersal and alterations in subcellular structures in the* Bbcal1 *mutant*

No obvious changes in growth and colony morphology were evident between the *Bbcal1* mutant and the wild-type parent on standard media including Sabouraud dex-trose containing 0.5% yeast extract (SDAY), potato dextrose agar (PDA) and Czapek-Dox plates (CZA), nor were any differences noted under various stress conditions including CZA supplemented with 2 mM ethyl-ene glycol tetraacetic acid (EGTA), 1.5 M KCl (salt/ osmotic stress), g ml^{-1} Congo red (cell wall stress) (Fig. S2). Conidial yield was unaffected on CZA plates, with a small initial (at 10 days) decrease seen on PDA plates that was no longer apparent by 15 or 20 days (Fig. 2). Conidiation of both the wild-type and *Bbcal1* strains on PDA plates supplemented with 1% C16 was reduced at the initial test time point (10 days), equivalent to PDA at 15 days, but did not increase any further (up until the 20-day time point). No significant differences in germination rates of conidia harvested from PDA plates were seen between the *Bbcal1* mutant and the wild-type parent. Microscopic examination of the growing mycelia and conidial production, however, revealed more compact assemblages of conidia in the *Bbcal1* mutant as compared with the wild type (Fig. 3A). Using a semi-quantitative spore dispersal assay as detailed in the Experimental procedures section, with capture plates ranging from 75 to 150 mm, an approximate 50% decrease in the dispersal of spores was seen (Fig. 3B).

Nile red was used to visualize LDs in the fungal cells. No obvious differences were seen in Nile red staining of conidia, or conidia germinating in potato dextrose broth (PDB) or on locust wings (Fig. S3). In order to examine subcellular structures in greater detail, fungal conidia har-vested from a variety of media including those supple-mented with lipids were examined using transmission electron microscopy. Wild-type *B. bassiana* conidia har-vested from PDA often containing numerous lipid bodies (Fig. 4A and Fig. 5A and B), and in some instances (1–2% of the cells), multilamellar ER-like structures were visible that were distinct from normal ER morphology [Fig. 4B and C, representative transmission electron microscopy (TEM) images of conidia are shown in the figures, in all cases > 100 conidia were

examined for each condition described below and a semi-quantitative assessment is given]. In contrast, > 90% of the *Bbcal1* mutant conidia harvested from PDA plates contained the multilamellar ER-like structures. In addition, multiple such structures were often visible within a single cell (Fig. 4D–H). In addition, some *Bbcal1* conidia (2–3%) contained large vesicles/vacuoles within which multilamellar structures could be seen, whereas others (2–3%) contained vacuoles containing dark granules (Fig. 4I). Conidia harvested from PDA plates supplemented with 1% olive oil contained increased amounts of LDs for both the wild-type and *Bbcal1* strain, although in the latter case, the multilamellar structures were again evident (Fig. 5E–H). Most wild-type conidia isolated from PDA + 1% oleic acid (OA) contained numerous vacuoles containing dark granules, and similar structures were seen in *Bbcal1* conidia, although within these, multilamellar structures were often found in the mutant conidia (Fig. 5I–L). Wild-type *B. bassiana* conidia harvested from PDA supplemented with 1% glyceride trioleate (GT) contained vacuole-like structures similar to those seen from cells grown in the presence of OA; however, they appeared smaller and did not contain as much electron-dense material as seen in the latter cells (Fig. 5M and N). *Bbcal1* conidia harvested from GT-supplemented plates also contained small vacuole-like structures, although these often contained large electron-dense granules (Fig. 5O and P). In addition, regions of small electron-dense material could be seen in these cells, often multiple in number and scattered throughout the cell, although membranous multilamellar structures (as seen in conidia harvested under other conditions) could not be discerned. For both the wild-type and mutant, as seen in cells harvested from olive oil-containing plates, numerous LDs could be seen, including some rather large in size. Fungal conidia isolated from PDA plates containing (1%) the alkane, C16, contained vacuole-like structures similar to those seen in cells grown in the presence of OA, and included small electron-dense granules; however, these structures were not as prevalent as seen for conidia grown on the other conditions examined (Fig. 5Q–T). Under similar conditions, few of the vacuole-like structures were seen in the *Bbcal1* mutant conidia, and fewer and smaller multilamellar structures or moderately electron-dense materials were seen as com-pared with *Bbcal1* conidia isolated from the other conditions examined.

A set of cellular lipid analyses was performed in order to determine any changes in lipid profiles of wild-type conidia grown in the presence of various lipid substrates as well as any alterations of such profiles in *Bbcal1* cells. Wild-type and *Bbcal1* conidia harvested from a variety of growth conditions were extracted and their lipid profiles analysed as detailed in the Experimental procedures section. In all instances, quantitative peak areas were determined, and the data were normalized to an internal standard as well as to cell number. Phosphatidylcholine (PC) analysis revealed 16 different species including two lysophosphatidylcholines (lysoPCs). For both wild-type and the mutant, a major peak at m/z = 782 (36:4), smaller peaks at m/z = 758 (34:2, 35:2) and 784 (36:3), as well as a number of additional minor components were noted in most media (Fig. 6A and B). Comparison of wild-type conidia harvested from different media revealed that on CZA or SDAY, wild-type cells contained 1.7–2-fold increase in the m/z 782 species and a four- to sixfold increase in the m/z 758 species, compared with cells grown in PDA. In addition, wild-type CZA conidia contained 4–10-fold increases in m/z species: 520 (lysoPC), 756 (34:3), 780 (36:5), 784 (36:3) and 786 (36:2), although many of these were minor components of the overall PC content. Growth on PDA + C16 resulted in a dramatic decrease of almost all PC content, with barely detectable amounts of the m/z 758, 782 and 784 species. Conidia analysed from PDA + OA showed similar PC profiles as PDA with the exception of elevated levels of the m/z 782 (36:4, 30% increase) and approximately twofold increase in the m/z 784 (36:3) species. Conidia harvested from PDA + GT contained approximately two- to threefold reduction in levels of m/z 758 (34:2, 35:2) and 782 (36:4), with little changes seen in the other species as compared with PDA isolated conidia. Loss of *Bbcal1* resulted in significant accumulation of PCs. Under all growth conditions, an enhancement of the major m/z 782 (36:4) species was seen (Fig. 6B). Comparisons of *Bbcal1* conidia harvested from different growth condi-tions, in general followed that seen for the wild-type, with a few notable exceptions. *Bbcal1* SDAY conidia contained the highest levels of m/z 758 (34:2, 35:2) and 782 (36:4) species, whereas PC content in *Bbcal1* CZA conidia more closely matched *Bbcal1* PDA conidia (unlike the situation seen for wild-type conidia). Perhaps the most easily visualized differences could be discerned in *Bbcal1* PDA + C16 derived conidia in which, although the major m/z peaks were suppressed,

significant amounts were still detected (unlike wild type) and the appearance of significant amounts of m/z 810*, 834, 836, as well as several others were clearly observable. In addition, *Bbcal1* OA and *Bbcal1* GT conidia were in general similar to *Bbcal1* PDA with few significant changes seen between these cells in contrast to wild type as described above.

Two species of phosphatidylethanolamine (PE) were detected in *B. bassiana*; m/z 716 (34:2) and 740 (36:4) (Fig. 7). Wild-type PDA conidia contained an approxi-mately twofold greater amount of the m/z 740 (36:4) species than the 716 (34:2). Wild-type conidia harvested from PDA + C16 were completely suppressed, whereas those isolated from PDA + GT contained an approxi-mately twofold decrease for both PE species. In contrast, wild-type conidia harvested from PDA + OA, CZA or SDAY contained 25% to fourfold increased amounts of the m/z 716 (34:2) and 740 (36:4) species. Conidia derived from *Bbcal1* PDA contained approximately twofold greater amounts of the m/z 716 (34:2) but similar levels of the 740 (36:4) species as wild type. No detectable amounts of PE were seen for *Bbcal1* PDA + C16 harvested conidia and decreasing amounts of the m/z 716 (34:2) were seen for *Bbcal1* PDA + OA, followed by PDA + GT and CZA; however, the concentration of this species of PE increased approximately twofold in conidia harvest from SDAY. With respect to the PE m/z 740 (36:4) species, increased levels were seen for *Bbcal1* PDA + OA and SDAY, and comparable levels were seen for PDA + GT and CZA derived conidia as compared with *Bbcal1* PDA conidia. Comparison with wild-type revealed decreased levels of both PE species on CZA but increased levels of both for mutant conidia harvested from PDA + GT plates. In addition, a ∼2.2-fold increase in only the m/z 716 (34:2) species was seen for *Bbcal1* PDA conidia as compared to wild-type PDA derived conidia.

Phytoceramide levels were 20% to twofold higher in *Bbcal1* conidia as compared to wild-type when har-vested from PDA, PDA + C16, PDA + OA and PDA + GT plates (Fig. 8). In contrast phytoceramide levels were similar between the two strains in conidia isolated from CZA and SDAY plates. For the wild-type, variation in phytoceramide levels between the various media was up to approximately threefold, whereas for the *Bbcal1* mutant the variation was only ∼30%. Dehydroergosterol levels were increased approximately twofold in *Bbcal1* PDA and *Bbcal1* PDA + GT

growth conditions as compared with wild type with comparable levels seen between the two strains in conidia derived from PDA + OA, CZA and SDAY (Fig. 9). Dehydroergosterol levels were signifi-cantly lower (5–15 fold) for both strains in conidia derived from PDA + C16 plates, with an approximately twofold dif-ference seen between the wild-type and *Bbcal1* strains.

Disruption of Bbca11 *affects pathogenicity*

Insect bioassays, using the greater wax moth, *G. mellonella* as the target host, were used to determine the effect of the *Bbcal1* mutant on virulence. Conidia of *B. bassiana* wild-type and the Bbcal1 mutant were adjusted to 2×10^7 spores $ml^{-1}$and applied topically, which represents the natural route of infection, to the larvae, and mortality was determined over a 9 day time-course (Fig. 10). These data showed an increased lethal time (LT50) to kill for the mutant as compared to the wild-type strain, where at day 4, the *Bbcal1* mutant displayed a 60% reduction in insect mortality as com-pared with the wild-type parent (~19% total mortality versus 48%). The calculated LT50 values were as follows (in days): wild type = 4.1 ± 0.13 and *Bbcal1* mutant = 5.5 ± 0.2. Aside from the reduced virulence no other obvious defects in disease progression were noted and the mutant strain was able to sporulate on the host cadaver essentially like the wild-type parent.

Discussion

The ability to store fatty acids and neutral lipids in LDs is an evolutionary highly conserved process seen in bacte-ria, fungi, plants and animals. Such sequestration of lipids provides the capacity for storage of energy reservoirs for future use and limits potential toxic chemical reactions that free or excess fatty acids and other lipids can undergo; the latter, a phenomenon termed ‘lipotoxicity’, can result in cell damage and/or death (apoptosis) and has been linked to a variety of cellular and organismal pathologies (Le Lay and Dugail, 2009; Vigouroux *et al.*, 2011). Lipid storage and the formation of LDs is a dynamic process reflecting exogenous lipid uptake and *de novo* lipid synthesis versus lipid consumption. LDs form via accumulation and budding of neutral lipids surrounded by a phospholipid monolayer from the ER,

during which various proteins are also inserted into the membrane. LDs may also 'grow' via cytoplasmic fission events, and they have also been implicated in regulating aspects of their originating organelle (the ER) affecting ER homeostasis and potentially ER stress-related pathologies (Hapala *et al*., 2011).

A wide variety of lipolytic bacteria and fungi have been described, and the enzymes derived from these organ-isms are of great interest in various biotechnological appli-cations (Thomson *et al*., 1999; Fickers *et al*., 2005; Joshi and Vinay, 2007). Lipid assimilation has been linked to microbial virulence; e.g. *Mycobacterium tuberculosis* accumulates lipids originating from the host as well as via *de novo* synthesis that is re-activated during infection and disease progression (Cotes *et al*., 2008), and various fungi, e.g. *Cryptococcus neoformans*, secrete extracellular lipases that contribute to survival, coloniza-tion and penetration of host tissues (Park *et al*., 2013). The oleaginous yeast, *Yarrowia lipolytica*, capable of uti-lizing a range of hydrophobic substrates including alkanes, fatty aids, fats and oils, represents a model system in which lipid assimilation has been studied (Fickers *et al*., 2005). Pathways for hydrocarbon uptake, storage and degradation, as well as specific transcription factors that regulate these processes, have been described in *Y. lipolytica* (Mauersberger *et al*., 2001; Thevenieau *et al*., 2007; Hirakawa *et al*., 2009). In addi-tion, metabolic and lipidomic profiling have provided clues as to how this yeast accumulates significant amounts of lipids (LDs) (Pomraning *et al*., 2015).

The outermost layer of the insect epicuticle, sometimes referred to as the waxy layer, consists of hydrocarbons including abundant amounts of long-chain alkanes and alkane derivatives, interspersed with fatty acids and wax esters. The waxy layer has been implicated in reducing water loss, as a platform for semiochemicals (compounds that function in insect communication), and as a protective coating against microbes (Ortiz-Urquiza and Keyhani, 2013). The ability to assimilate and/or detoxify specific cuticular compounds has been shown to entail a co-evolutionary arms race between *B. bassiana* and certain insects (Pedrini *et al*., 2015). In the insect patho-genic fungus, *M. anisopliae*, the ability of the fungus to mobilize lipid stores has been shown to be crucial for establishing the turgor pressure in the appressorial-infection structures needed for penetration of the stiff cuticle of the host (Wang and Leger, 2007). Pathways for alkane assimilation by *B. bassiana*, including its ability to grow on long-chain

alkanes (up to and perhaps beyond C33) and a suite of cytochrome P450s that can hydroxylate hydrocarbons mediating catabolism, have been described (Pedrini *et al*., 2010; 2013; Zhang *et al*., 2012). Regula-tion of OA and palmitic acid production has been linked to stress resistance and virulence in *Candida parapsilosis* (Nguyen *et al*., 2011) and fatty acid beta-oxidation pathways have been shown to affect virulence in *Cryptococcus neoformans* and in the fungal plant patho-gen, *Ustilago maydis* (Kretschmer *et al*., 2012a,b). However, although assimilation and/or detoxification of insect host hydrocarbons and fatty acids is known to be important for entomopathogenic fungi, little is known about lipid storage structures in *B. bassiana* and any alterations in lipid profiles during growth on various hydrocarbon substrates, i.e. on OA, GT, C16 and other lipids.

Genomic analysis indicated a single caleosin homo-logue in fungi, and the function of this gene and its protein product was investigated in *B. bassiana* via construction of a targeted gene knockout mutant. In general, the phenotypes of the *Bbcal1* strain were rather mild. No obvious phenotypes in growth in standard media or media supplemented with hydrocarbons was noted, and no effects were seen under various stress conditions includ-ing growth under high osmolarity or susceptibility to the cell wall stress agent Congo red. Vegetative growth and conidiation was apparently similar between the *Bbcal1* mutant and wild type; however, microscopic examination of growing fungal mycelia on agar plates revealed the production of tighter assemblages or clumping of conidia as compared with the wild-type parent. The formation of these structures was shown to impede the ability of the fungus to disperse, a likely critical environmental handi-cap that would not be readily apparent in laboratory growth assays. Although no obvious differences were seen in Nile red staining of LDs between the wild-type and *Bbcal1* conidia, TEM imaging of conidia harvested from standard media and media supplemented with either olive oil, OA, GT or C16 revealed significant alterations in differ-ent subcellular structures. In PDA, *Bbcal1* conidia accu-mulated a number of vesicle-like structures. These included electron-dense multilamellar and vacuole-like structures, some of the latter containing multilamellar bodies. Although the origins of the multilamellar bodies seen in *Bbcal1* conidia remain unclear, they could be derived from ER-(stress) or incorrect budding of LDs from the ER due to the lack of the caleosin protein. In addition,

although speculative, the accumulation of the multilamellar bodies could be due to reduced turnover, as a small percentage of these structures were seen in wild-type cells. In *Arabidopsis*, loss of the *AtCLO1* caleosin, one of five such genes found in this organism, delayed LD breakdown during seed germination, and an interaction between LDs and vacuoles during degradation of storage lipid was noted (Poxleitner *et al*., 2006). This would be consistent with a role for the *B. bassiana* caleosin in medi-ating turnover of lipid-associated structures.

Accumulation of aberrant cellular substructures was seen for *Bbcal1* conidia derived from a variety of lipid growth substrates, although the morphology of these structures differed (in both wild-type and the mutant) depending upon the lipid substrate added. Consistent with increases in apparent multilamellar vesicle-like mem-brane structures, i.e. greater membrane content, lipid analyses indicated increased amounts of PC and PE in mutant conidia compared with wild type during growth on PDA. Growth on PDA + olive oil resulted in conidia with abundant LDs for both the wild-type and *Bbcal1* conidia, with additional electron-dense material seen in the mutant strain. Although unlike PDA-derived conidia, clear obser-vations of multilamellar structures were not evident. Conidia isolated from PDA + OA contained abundant and sometimes very large LDs along with vacuole-like bodies with electron-dense granules that were more numerous and larger in *Bbcal1* conidia compared with wild type, and in many instances multilamellar structures could be discerned as part of these. Cells grown on OA also showed slightly elevated amounts (compared with PDA conidia) of PC, PE, ceramide and ergosterol. Similar levels of PE were seen in these cells, however, a decrease in PC, and elevated levels of ceramide and ergosterol were seen for *Bbcal1* conidia compared to the wild-type. Ergosterol, the primary sterol found in fungal cell membranes but absent in plant and animal mem-branes (Pasanen *et al*., 1999), was also elevated in the conidia of the *B. bassiana* caleosin mutant. Recent evi-dence suggests that ergosterol may act as a fungal microbe-associated molecular pattern recognition mol-ecule potentially perceived by plant pattern recognition receptors (Klemptner *et al*., 2014). One can speculate that increased ergosterol levels may result in greater stimulation of host defences and may be one factor in the decreased virulence seen in the *B. bassiana* caleosin mutant. Ceramides are important regulators of cell devel-opment,

differentiation and stress response. Some ceramides act as secondary messengers affecting the activities of both protein kinase and phosphatase cas-cades (Ruvolo, 2003). In *Saccharomyces cerevisiae*, elevation of the soluble C2-phytoceramide results in inhi-bition of cell proliferation and integrity, perturbing lipid raft formation (Pacheco *et al*., 2013). In contrast, loss of the C18:1-phytoceramide in yeast results in hydroxyurea sensitivity (Matmati *et al*., 2013), and ceramide synthase was isolated using a screen for resistance to fumonisin B1, the latter a fungal toxin that inhibits cell growth via suppression of sphingolipid biosynthesis (Mao *et al*., 2000). Fatty acids are known to display antifungal activity against phytopathogenic and other fungi (Liu *et al*., 2008), and a cytochrome P450 mediated pathway has recently been characterized in the bark beetle-associated fungus, *Grosmannia clavigera* that likely plays a role in detoxification and utilization of pine triglycerides of which OA is the most common fatty acid (Novak *et al*., 2015). Similarly, the ability of *B. bassiana* to grow and/or detoxify fatty acids can have a direct impact of its ability to parasitize insect hosts. In general, *Bbcal1* conidia contained more numerous electron-dense bodies than wild-type, with the exception of those harvest from PDA plates supplemented with C16, which contained far fewer such structures in both the wild-type and mutant cells. Surprisingly (but consistent with the TEM visualization), lipid content was significantly sup-pressed during growth on C16-supplemented media particularly for the wild-type in which PC and PE levels could barely be detected, and ergosterol levels were decreased by ~85%, although ceramide levels were unaf-fected. PC and PE levels were also dramatically reduced in *Bbcal1* C16 conidia, although the accumulation of previously low-level PC species was noted. Ergosterol levels, while twice that of wild type, were ~85% of *Bbcal1* PDA conidia, following the same trend as the wild type. Simi-larly, for *Bbcal1* C16 conidia, ceramide levels were unaf-fected, more than twice that of wild-type and higher than *Bbcal1* PDA conidia. Furthermore, PC accumulation was highest for both the wild-type and *Bbcal1* conidia on CZA and SDAY media, with levels in the mutant on SDAY almost twice that of the wild type. In most cases similar (and high, relative to the other conditions examined) levels of PE, ceramide and ergosterol were seen for wild-type and *Bbcal1* conidia harvested from CZA and SDAY.

Taken together, our data reveal dynamic lipid profiles for conidia harvested under a variety of conditions, includ-ing standard ones used to produce conidia for insect control purposes. It has previously been shown that growth on insect hydrocarbons can 'prime' *B. bassiana* for increased virulence (Crespo *et al*., 2002), and our data may help account for variation in infectivity of fungal conidia harvested from different media and used in bio-logical control applications. These data support the idea that variation in lipid content and hence adaption to exog-enous lipid (e.g. induction or accumulation of lipases and lipid detoxifying enzymes) and/or the ability to mobilize lipids for successful infection, are dependent upon the fungal growth substrata used to produce the conidia. Importantly, no significant changes were seen in conidial germination and/or the various stress conditions tested. This differs from apparent role(s) of caleosins in plants, in which these proteins have been implicated in seed ger-mination and stress response. Our data provide the first glimpse into the functions of caleosins in fungi, linking these proteins to virulence in a fungal pathogen. However, given the potential importance of the caleosin in contrib-uting to cellular lipid balance, it is somewhat surprising that the effect on virulence was rather small. These data suggest potential compensatory effects and/or partners in LD development, maintenance, and use in these fungi. Further exploration of the physiological roles of caleosins, their interacting partners and contributions to lipid homeo-stasis in fungi is warranted.

Experimental procedures

Chemical reagents and cultivation of fungi

Beauveria bassiana (ATCC 90517) was routinely grown on PDA, CZA and SDAY. Plates were incubated at 26°C for 10–14 days and aerial conidia were harvested by flooding the plate with sterile distilled H_2O. Conidial suspensions were filtered through a single layer of Miracloth and final spore concentrations were determined by direct count using a haemocytometer (OLYMPUS BX41, 40×). For growth on lipid substrates, PDA was supplemented with either 0.25% OA, 0.5% GT, or 0.2% alkane prepared in hexane at a concen-tration of 10% and added to the media immediately prior to pouring of the plates.

Nucleic acid manipulations and construction of Bbcal1 *strains*

To generate the vector for construction of the *Bbcal1* knock-out strain in *B. bassiana* via homologous recombination, 856 bp of LB and 816 bp of RB nucleotide sequence for *Bbcal1* were obtained by PCR using primer pairs PcaL1/L2 and PcaR1/R2. Primers PBar1 and PBar2 were used to amplify the *bar* (phosphinothricin resistance) marker cas-sette; PcaL2 and PcaR1 were chimeric primers containing a short stretch of *bar* cassette sequences at their 5′ ends and a short region of the *Bbcal1* sequence at their 3′ ends. PCR fragments corresponding to the LB, *bar* and RB were assem-bled together by primerless PCR as previously described (Fan *et al*., 2012a). The LB-*bar*-RB fragment was amplified by primers PcaL1 and PcaR2 and cloned into the pDrive vector and the integrity of the insert was verified by sequenc-ing (UF ICB-CORE). Preparation of competent cells, trans-formation, screening of recombinant clones and genomic DNA preparation were performed essentially as described (Zhang *et al*., 2010; Fan *et al*., 2011). The transformation mixture (0.25–0.5 ml) was plated onto Czapek-Dox medium containing 200 μg ml^{-1} phosphinothricin, 0.01% bromocresol purple, pH 6.3, in 150 mm diameter Petri dishes overlaid with a sheet of sterilized cellophane. Putative gene knock mutants were screened and verified by PCR analysis using primers Pcal-t1 and Pcal-t2 designed to the 5′ and 3′ flanking regions of the *Bbcal1* gene. PCR reactions were performed using the following protocol: 95°C for 3 min, followed by 35 cycles of denaturation at 95°C for 30 s, annealing at 56°C for 30 s, and extension at 72°C for 1 min. Fungal genomic DNA for PCR analysis was isolated as follows; a small amount of mycelia was picked from the colony into 8 μl 0.3 M sodium hydroxide solution in a 200 μl PCR tube with a toothpick. After incubat-ing the PCR tube at 95°C for 1 min in a PCR instrument, 160 μl 20 mM Tris–HCl (pH 8.0) and 8 μl 0.3 M HCl were added to neutralize the solution. The extract (1–3 μl) contain-ing fungal genomic DNA was used as the template for PCR analysis. The complementation vector, pSUR-*Bbca11*, was constructed using the entire open reading frame, along with 1.8 kb of LB and 183 bp of RB flanking sequences This region was amplified from using *B. bassiana* genomic DNA as the template and primers Pcal1/Pcal2. The product was cloned into pCB1536 that contains the selection marker for sulfonylurea resistance. Transformation of pSUR-*Bbcal1* into *B. bassiana Bbca11* was performed as

described previously and putative transformants isolated on CZA supplemented with 10 μg ml^{-1} sulfonylurea (Zhang *et al*., 2010). The integ-rity of the transformants was confirmed by PCR and Southern blotting. PCR confirmation was performed on genomic DNA extracted from transformants using primers Pcal-t1 and Pcal-t2. Southern blotting was performed using 10 μg genomic DNA digested with *Eco*RI. The digested DNA was separated in 1.0% agarose gel and subsequently transferred to Biodyne B nylon membrane (Gelman Laboratory, Shelton, WA, USA) using standard protocols. Blots were probed with a 400 bp PCR amplified product corresponding to gDNA, generated using the PcaL1 and Pcal-S primers. Probe preparation, membrane hybridization and visualization were performed using DIG High Prime DNA Labeling and Detection Starter Kit I (Roche).

RNA isolation and real-time PCR

Expression of *Bbcal1* was investigated during growth in sabouraud dextrose broth (SDB) broth and PDA agar medium. The cultures were harvested at various time points, after which the total RNA was extracted using RNA Easy Kit (Qiagen) following the manufacturer's instructions. After treating the samples with DNase (Ambion), cDNA was gen-erated using the AffinityScript multiple temperature cDNA synthesis kit (Stratagene). Real-time PCR was performed using an ABI 7000 thermocycler (Applied Biosystems) and the reaction products were detected with SYBR Green (BioRad). PCR was accomplished after a 10 min denatura-tion step at 95°C, followed by 40 cycles of 30 s at 95°C, 30 s at 56°C and 30 s at 72°C. Fluorescence was detected and recorded at each polymerization step. The relative expres-sion of *Bbcal*1 was normalized against *tubulin*, *actin* and *gpd* as the reference genes, using geNORM (Vandesompele *et al*., 2002). Primers are listed in Table S1.

Phenotypic assays

Fungal growth under various conditions was examined as follows; 1 μl conidial suspension (5×10^6 conidia ml^{-1}) was spot inoculated on test plates, and all the plates were incu-bated at 26°C and observed daily over 3–10 days, with radial growth quantified. Test plates included: CZA, CZA supple-mented with 2 mM EGTA and the pH indicator bromocresol purple (0.01%), PDA and PDA supplemented with either 1.5 M KCl, 1.5 M sorbitol, or 100 μg ml^{-1} Congo red. Conidiation was

examined by spreading a lawn of conidia (50 µl 5 × 10^6 conidia ml^{-1}) on test plates (90 mm diameter) including CZA, PDA and PDA + hexadecane (C_{16}, 30 µl of 10% solution in hexane/each plate). Plates were incubated at 26°C, > 75% relative humidity and at indicated time points (10, 15 and 20 days) 0.5 cm diameter fungal discs were removed with a bore from each plate. Fungal discs placed in glass test tubes were immersed in 1 ml of sterile dH_2O + 0.05% Tween-80 and shaken for 5 min. Total conidia was directly counted using a haemocytometer. For Nile red stain-ing, freshly harvested conidia and fungal conidia grown (ger-minating conidia) in PDB for 14 h or on locust wings for 24 h were isolated. Harvested fungal cells were fixed in 3% for-maldehyde for 2 h and then stained with 0.5 µg ml^{-1} Nile red for 5 min, then washed with PBS (pH 7,0) for two times. Mounted slides were observed using a PASCAL LMS5 con-focal microscope. Fungal spore dispersal was assayed as follows; agar media were poured into both the top and bottoms of Petri plates (90–150 mm). Agar (1.5%) was poured onto one side (designed as the top plate), and SDAY medium was poured into the other (i.e. the lid and designed as dispersal plate). The SDAY agar on the dispersal plates was trimmed along the edges removing ∼2–4 mm ring around the edge of the plate. A lawn of fungal conidia was spread onto the top plate (100–150 µl, 1 × 10^7 conidia ml^{-1}), and the plates were incubated with the lawn side facing down at 26°C. Colonies formed on the dispersal plate was observed after 10–15 days.

Microscopy

Samples for TEM were prepared as follows: conidial cells harvested from various growth conditions were centri-fuged to pellet (10 000 r.p.m., 5 min) and fixed with 2% glutaraldehyde, 4% paraformaldehyde in 0.1 M sodium cacodylate buffer, pH 7.2 and stored at 4°C overnight. Fixed cells were processed with the aid of a Pelco BioWave laboratory microwave. The samples were washed in 0.1 M sodium cacodylate pH 7.24, post-fixed with 2% buffered osmium tetroxide, water washed and dehydrated in a graded ethanol series 25%, 50%, 75%, 95%, 100%, followed by 100% acetone. Dehydrated samples were infiltrated in graded acetone/Spurrs epoxy resin and cured at 60°C. Cured resin blocks were trimmed, thin sectioned and collected on Formvar copper slot grids, post-stained with 2% aqueous uranyl acetate and Reynolds' lead citrate. Sections were examined with a Hitachi H-7000 TEM

and digital images were acquired by using a Veleta camera and iTEM software. At least two independent batches of fungal conidia were examined for all samples.

Lipid analysis

Fungal conidia were harvested from various growth condi-tions including: CZA, SDAY, PDA and PDA supplemented with either 0.25% OA, 0.5% GT or 0.2% alkane (prepared in hexane at a concentration of 10%). All the plates were cul-tured at 26°C for 30 days before harvesting of conidia. The conidia were harvested in sterilized H_2O and 10^8–10^9 conidia were used for lipid profiles analysis. Conidia were extracted using the Folch method. Briefly, 30 μl of a 10 μg ml^{-1} solution of dilaurylphosphatidylcholine (internal standard) was added, then 1 ml of 2:1 Chloroform:methanol containing 100 mg l^{-1} of butylated hydroxytoluene was added to each sample and mixed. The samples were centrifuged at 10 000 × *g* and the supernatant was transferred to a new tube. Next, 200 μl of 0.9% NaCl was added to induce phase separation. After mixing and gentle centrifugation (3000 r.p.m.), the chloroform layer was removed and transferred to a clean tube. The extraction process was repeated once on the pellet and the chloroform layers were combined. The combined mixture was dried under a gentle stream of nitrogen. The dried samples were then reconstituted with 300 μl of 48:26:14:12 isopropanol with 5 mM ammonium formate and 0.1% formic acid:methanol:chloroform:water with 5 mM ammonium formate and 0.1% formic acid. Ten microlitres were injected for liquid chromatography tandem mass spectroscopy (LC-MS/MS) analysis.

LC-MS/MS analysis was performed on a Thermo TSQ Quantum Ultra with Accela 1000 UHPLC and autosampler. The mass spectrometer was operated in positive heated electrospray ionization mode with the following conditions: 3.5 kV, 50°C probe temperature, 35 arb sheath gas, 30 arb aux gas, 1.0 ion sweep gas and 320°C heated capillary temperature. Precursor ion scanning was used for PC and sphingomyelin (SM) monitoring *m/z* 184.1 with a collision energy of 35, neutral loss scanning was used for PE moni-toring *m/z* 141.3 with a collision energy of 30, and precursor ion scanning was used for ceramides monitoring *m/z* 264.1 with a collision energy of 30 V. The collision gas (argon) pressure was 0.7 mTorr for all experiments. Separation was achieved on an Accucore RP-MS 30 × 2.1 mm, 2.6 μm

(Thermo) column with mobile phase A as 0.1% formic acid in water and mobile phase B as methanol under gradient elution conditions (0–0.5 min 80%B, 0.5–5 min 90%B, 5–9 min 100%B, 9–11 min 100%B, 11–16 min 100%B, 16.5 min 80%B, 20 min 80%B). The flow rate was 250 μl min^{-1} except from 11–16 min where the flow rate was increased to 300 μl min^{-1}.

Insect bioassays

Fungal virulence bioassay was performed using *G. mellonella* larvae (Pet Solutions, Dayton, OH, USA). The larvae were dipped for 5–10 s in solutions of 2×10^7 conidia ml^{-1} harvested in sterile Tween-80 (0.05%), and the excess liquid on the insect bodies removed by placement on dry paper towel. Controls were treated with sterile Tween-80. Experimental and control larvae were placed in plastic cham-bers or large (150 mm) Petri dishes and were incubated at 26°C. For each experimental condition, 20–40 larvae were used, and all experiments were repeated three times. The number of dead insects was recorded daily and median LT_{50} was calculated by probit analysis.

Gene sequences

The *B. bassiana* DNA sequence corresponding to *Bbcal1* has been deposited in GenBank under the accession numbers XM_008602402.1 (nucleotide sequence) and EJP63661 (protein sequence). Analysis of the isolated nucleotide sequences was performed via the NCBI BLAST portal. Protein alignments were performed using CLUSTAL X.

Acknowledgements

This material is based upon work that is supported by the National Institute of Food and Agriculture, U.S. Department of Agriculture, under award number 2010-34135-21095 and a National Science Foundation grant (IOS-1121392) to NOK. The authors wish to thank Dr. B.-H. Kang and K. Kelley (UF-ICBR Microscopy Facility) for assistance with the electron microscopy.

References

Abell, B.M., Holbrook, L.A., Abenes, M., Murphy, D.J., Hills, M.J., and Moloney, M.M. (1997) Role of the proline knot motif in oleosin endoplasmic reticulum topology and oil body targeting. *Plant Cell* **9:** 1481–1493.

Aubert, Y., Vile, D., Pervent, M., Aldon, D., Ranty, B., Simonneau, T., *et al*. (2010) RD20, a stress-inducible caleosin, participates in stomatal control, transpiration and drought tolerance in *Arabidopsis thaliana*. *Plant Cell Physiol* **51:** 1975–1987.

Bickel, P.E., Tansey, J.T., and Welte, M.A. (2009) PAT pro-teins, an ancient family of lipid droplet proteins that regulate cellular lipid stores. *Biochim Biophys Acta* **1791:** 419– 440.

Chapman, K.D., Dyer, J.M., and Mullen, R.T. (2012) Biogenesis and functions of lipid droplets in plants. *J Lipid Res* **53:** 215–226.

Chen, J.C.F., Tsai, C.C.Y., and Tzen, J.T.C. (1999) Cloning and secondary structure analysis of caleosin, a unique calcium-binding protein in oil bodies of plant seeds. *Plant Cell Physiol* **40:** 1079–1086.

Cho, E.M., Boucias, D., and Keyhani, N.O. (2006a) EST analysis of cDNA libraries from the entomopathogenic fungus *Beauveria (Cordyceps) bassiana*. II. Fungal cells sporulating on chitin and producing oosporein. *Microbiol-ogy* **152:** 2855–2864.

Cho, E.M., Liu, L., Farmerie, W., and Keyhani, N.O. (2006b) EST analysis of cDNA libraries from the entomopathogenic fungus *Beauveria* (*Cordyceps*) *bassiana*. I. Evidence for stage-specific gene expression in aerial conidia, in vitro blastospores and submerged conidia. *Microbiology* **152:** 2843–2854.

Cotes, K., N'Goma, J.C.B., Dhouib, R., Douchet, I., Maurin, D., Carriere, F., and Canaan, S. (2008) Lipolytic enzymes in *Mycobacterium tuberculosis*. Appl Microbiol Biotechnol **78:** 741–749.

Crespo, R., Juarez, M.P., Dal Bello, G.M., Padin, S., Fernandez, G.C., and Pedrini, N. (2002) Increased mortality of *Acanthoscelides obtectus* by alkane-grown *Beauveria bassiana*. *Bio Control* **47:** 685–696.

Fan, Y., Zhang, S., Kruer, N., and Keyhani, N.O. (2011) High-throughput insertion mutagenesis and functional screening in the entomopathogenic fungus *Beauveria bassiana*. *J Invertebr Pathol* **106:** 274–279.

Fan, Y., Ortiz-Urquiza, A., Kudia, R.A., and Keyhani, N.O. (2012a) A fungal homologue of neuronal calcium sensor-1, *Bbcsa1*, regulates extracellular acidification and contributes to virulence in the entomopathogenic fungus *Beauveria bassiana*. *Microbiology* **158:** 1843–1851.

Fan, Y., Borovsky, D., Hawkings, C., Ortiz-Urquiza, A., and Keyhani, N.O. (2012b) Exploiting host molecules to augment mycoinsecticide virulence. *Nat Biotechnol* **30:** 35–37.

Fickers, P., Benetti, P.H., Wache, Y., Marty, A., Mauersberger, S., Smit, M.S., and Nicaud, J.M. (2005) Hydrophobic substrate utilisation by the yeast *Yarrowia lipolytica*, and its potential applications. *FEMS Yeast Res* **5:** 527– 543.

Frandsen, G.I., Mundy, J., and Tzen, J.T.C. (2001) Oil bodies and their associated proteins, oleosin and caleosin. *Physiol Plant* **112:** 301–307.

Glare, T., Caradus, J., Gelernter, W., Jackson, T., Keyhani, N., Kohl, J., *et al*. (2012) Have biopesticides come of age? *Trends Biotechnol* **30:** 250–258.

Greenberg, A.S., Coleman, R.A., Kraemer, F.B., McManaman, J.L., Obin, M.S., Puri, V., *et al*. (2011) The role of lipid droplets in metabolic disease in rodents and humans. *J Clin Invest* **121:** 2102–2110.

Hapala, I., Marza, E., and Ferreira, T. (2011) Is fat so bad? Modulation of endoplasmic reticulum stress by lipid droplet formation. *Biol Cell* **103:** 271–285.

He, Z., Zhang, S., Keyhani, N.O., Song, Y., Huang, S., Pei, Y., and Zhang, Y. (2014) A novel mitochondrial membrane protein, Ohmm, limits fungal oxidative stress resistance and virulence in the insect fungal pathogen *Beauveria bassiana*. *Environ Microbiol*.

Hirakawa, K., Kobayashi, S., Inoue, T., Endoh-Yamagami, S., Fukuda, R., and Ohta, A. (2009) Yas3p, an Opi1 family transcription factor, regulates cytochrome P450 expression in response to n-alkanes in *Yarrowia lipolytica*. J Biol Chem 7126–7137.

Holder, D.J., and Keyhani, N.O. (2005) Adhesion of the entomopathogenic fungus *Beauveria (Cordyceps) bassiana* to substrata. *Appl Environ Microbiol* **71:** 5260– 5266.

Joshi, G.K., and Vinay, S. (2007) Bacterial lipases: classifi-cation, properties and applications in biotechnology. *Res J Biotechnol* **2:** 50–56.

Kirkland, B.H., Westwood, G.S., and Keyhani, N.O. (2004) Pathogenicity of entomopathogenic fungi *Beauveria bassiana* and *Metarhizium anisopliae* to Ixodidae tick species *Dermacentor variabilis*, *Rhipicephalus sanguineus*, and *Ixodes scapularis*. *J Med Entomol* **41**: 705–711.

Klemptner, R.L., Sherwood, J.S., Tugizimana, F., Dubery, I.A., and Piater, L.A. (2014) Ergosterol, an orphan fungal microbe-associated molecular pattern (MAMP). *Mol Plant Pathol* **15:** 747–761.

Kretschmer, M., Klose, J., and Kronstad, J.W. (2012a) Defects in mitochondrial and peroxisomal beta-oxidation influence virulence in the maize pathogen *Ustilago maydis*. *Eukaryot Cell* **11:** 1055–1066.

Kretschmer, M., Wang, J., and Kronstad, J.W. (2012b) Peroxisomal and mitochondrial beta-oxidation pathways influence the virulence of the pathogenic fungus *Cryptococcus neoformans*. Eukaryot Cell 11: 1042–1054.

Le Lay, S., and Dugail, I. (2009) Connecting lipid droplet biology and the metabolic syndrome. *Prog Lipid Res* **48:** 191–195.

Lewis, M.W., Robalino, I.V., and eyhani, N.O. (2009) Uptake of the fluorescent probe FM4-64 by hyphae and haemolymph-derived *in vivo* hyphal bodies of the entomopathogenic fungus *Beauveria bassiana*. *Microbiology* **155:** 3110–3120.

Lin, I.P., Jiang, P.L., Chen, C.S., and Tzen, J.T.C. (2012) A unique caleosin serving as the major integral protein in oil bodies isolated from *Chlorella* sp cells cultured with limited nitrogen. *Plant Physiol Biochem* **61:** 80–87.

Liu, S.Y., Ruan, W.B., Li, J., Xu, H., Wang, J.G., Gao, Y.B., and Wang, J.G. (2008) Biological control of phytopathogenic fungi by fatty acids. *Mycopathologia* **166:** 93–102.

Mao, C.G., Xu, R.J., Bielawska, A., and Obeid, L.M. (2000) Cloning of an alkaline ceramidase from *Saccharomyces cerevisiae* – an enzyme with reverse (CoA-independent) ceramide synthase activity. *J Biol Chem* **275:** 6876– 6884.

Matmati, N., Metelli, A., Tripathi, K., Yan, S.Q., Mohanty, B.K., and Hannun, Y.A. (2013) Identification of C-18:1-phytoceramide as the candidate lipid mediator for hydroxyurea resistance in yeast. *J Biol Chem* **288:** 17272– 17284.

Mauersberger, S., Wang, H.J., Gaillardin, C., Barth, G., and Nicaud, J.M. (2001) Insertional mutagenesis in the n-alkane-assimilating yeast *Yarrowia lipolytica*: generation of tagged mutations in genes involved in hydrophobic sub-strate utilization. *J Bacteriol* **183:** 5102–5109.

Nguyen, L.N., Gacser, A., and Nosanchuk, J.D. (2011) The stearoyl-coenzyme A desaturase 1 is essential for virulence and membrane stress in *Candida parapsilosis* through unsaturated fatty acid production. Infect Immun 136–145.

Novak, M., Lah, L., Sala, M., Stojan, J., Bohlmann, J., and Komel, R. (2015) Oleic acid metabolism via a conserved cytochrome P450 system-mediated omega-hydroxylation in the bark beetle-associated fungus *Grosmannia clavigera*. *PLoS ONE* **10** (3)**:** e0120119.

Ortiz-Urquiza, A., and Keyhani, N.O. (2013) Action on the surface: entomopathogenic fungi versus the insect cuticle. *Insects* **4:** 357–374.

Ortiz-Urquiza, A., and Keyhani, N.O. (2015) Stress response signaling and virulence: insights from entomopathogenic fungi. *Curr Genet* **61:** 239–249.

Pacheco, A., Azevedo, F., Rego, A., Santos, J., Chaves, S.R., Corte-Real, M., and Sousa, M.J. (2013) C2-Phytoceramide perturbs lipid rafts and cell integrity in *Saccharomyces cerevisiae* in a sterol dependent manner. *PLoS ONE* **8** (9)**:** e74240.

Park, M., Do, E., and Jung, W.H. (2013) Lipolytic enzymes involved in the virulence of human pathogenic fungi. *Mycobiology* **41:** 67–72.

Partridge, M., and Murphy, D.J. (2009) Roles of a membrane-bound caleosin and putative peroxygenase in biotic and abiotic stress responses in *Arabidopsis*. *Plant Physiol Biochem* **47:** 796–806.

Pasanen, A.L., Yli-Pietila, K., Pasanen, P., Kalliokoski, P., and Tarhanen, J. (1999) Ergosterol content in various fungal species and biocontaminated building materials. *Appl Environ Microbiol* **65:** 138–142.

Pasaribu, B., Lin, I.P., Tzen, J.T.C., Jauh, G.Y., Fan, T.Y., Ju, Y.M., et al. (2014) SLDP: a novel protein related to caleosin is associated with the endosymbiotic Symbiodinium lipid droplets from *Euphyllia glabrescens*. Mar Biotechnol (NY) 560–571.

Pedrini, N., Zhang, S.Z., Juarez, M.P., and Keyhani, N.O. (2010) Molecular characterization and expression analysis of a suite of cytochrome P450 enzymes implicated in insect hydrocarbon degradation in the entomopathogenic fungus *Beauveria bassiana*. Microbiology 156: 2549–2557.

Pedrini, N., Ortiz-Urquiza, A., Huarte-Bonnet, C., Zhang, S., and Keyhani, N.O. (2013) Targeting of insect epicuti-cular lipids by the entomopathogenic fungus *Beauveria bassiana*: hydrocarbon oxidation within the context of a host-pathogen interaction. *Front Microbiol* **4:** 24.

Pedrini, N., Ortiz-Urquiza, A., Huarte-Bonnet, C., Fan, Y., Juarez, M.P., and Keyhani, N.O. (2015) Tenebrionid secretions and a fungal benzoquinone oxidoreductase form competing components of an arms race between a host and pathogen. *Proc Natl Acad Sci USA* **112:** E3651– E3660. doi:10.1073/pnas.1504552112.

Pol, A., Gross, S.P., and Parton, R.G. (2014) Biogenesis of the multifunctional lipid droplet: lipids, proteins, and sites. *J Cell Biol* **204:** 635–646.

Pomraning, K.R., Wei, S.W., Karagiosis, S.A., Kim, Y.M., Dohnalkova, A.C., Arey, B.W., *et al*. (2015) Comprehen-sive metabolomic, lipidomic and microscopic profiling of *Yarrowia lipolytica* during lipid accumulation identifies targets for increased lipogenesis. *PLoS ONE* **10** (4)**:** e0123188.

Poxleitner, M., Rogers, S.W., Samuels, A.L., Browse, J., and Rogers, J.C. (2006) A role for caleosin in degradation of oil-body storage lipid during seed germination. *Plant J* **47:** 917–933.

Ruvolo, P.P. (2003) Intracellular signal transduction pathways activated by ceramide and its metabolites. *Pharmacol Res* **47:** 383–392.

Sztalryd, C., and Kimmel, A.R. (2014) Perilipins: lipid droplet coat proteins adapted for tissue-specific energy storage and utilization, and lipid cytoprotection. *Biochimie* **96C:** 96–101.

Thevenieau, F., Le Dall, M.T., Nthangeni, B., Mauersberger, S., Marchal, R., and Nicaud, J.M. (2007) Characterization of *Yarrowia lipolytica* mutants affected in hydrophobic sub-strate utilization. *Fungal Genet Biol* **44:** 531–542.

Thomson, C.A., Delaquis, P.J., and Mazza, G. (1999) Detection and measurement of microbial lipase activity: a review. *Crit Rev Food Sci Nutr* **39:** 165–187.

Umate, P. (2012) Comparative genomics of the lipid-body-membrane proteins oleosin, caleosin and steroleosin in magnoliophyte, lycophyte and bryophyte. *Genomics Proteomics Bioinformatics* **10:** 345–353.

Vandesompele, J., De Preter, K., Pattyn, F., Poppe, B., Van Roy, N., De Paepe, A., and Speleman, F. (2002) Accurate normalization of real-time quantitative RT-PCR data by geometric averaging of multiple internal control genes. *Genome Biol* **3:** research0034.1-0034.11.

Vigouroux, C., Caron-Debarle, M., Le Dour, C., Magre, J., and Capeau, J. (2011) Molecular mechanisms of human lipodystrophies: from adipocyte lipid droplet to oxidative stress and lipotoxicity. *Int J Biochem Cell Biol* **43:** 862– 876.

Wanchoo, A., Lewis, M.W., and Keyhani, N.O. (2009) Lectin mapping reveals stage-specific display of surface carbohy-drates in *in vitro* and haemolymph-derived cells of the entomopathogenic fungus *Beauveria bassiana*. *Microbiology* **155:** 3121–3133.

Wang, C.S., and Leger, R.J.S. (2007) The *Metarhizium anisopliae* perilipin homolog *MPL1* regulates lipid metabolism, appressorial turgor pressure, and virulence. *J Biol Chem* **282:** 21110–21115.

Zhang, S., Fan, Y., Xia, Y.X., and Keyhani, N.O. (2010) Sulfonylurea resistance as a new selectable marker for the entomopathogenic fungus *Beauveria bassiana*. *Appl Microbiol Biotechnol* **87:** 1151–1156.

Zhang, S., Widemann, E., Bernard, G., Lesot, A., Pinot, F., Pedrini, N., and Keyhani, N.O. (2012) CYP52X1, repre-senting new cytochrome P450 subfamily, displays fatty acid hydroxylase activity and contributes to virulence and growth on insect cuticular substrates in entomopathogenic fungus *Beauveria bassiana*. *J Biol Chem* **287:** 13477– 13486.

Zhang, S.Z., Xia, Y.X., Kim, B., and Keyhani, N.O. (2011) Two hydrophobins are involved in fungal spore coat rodlet layer assembly and each play distinct roles in surface interactions, development and pathogenesis in the entomopathogenic fungus, *Beauveria bassiana*. *Mol Microbiol* **80:** 811–826.

Zienkiewicz, K., Zienkiewicz, A., Rodriguez-Garcia, M.I., and Castro, A.J. (2011) Characterization of a caleosin expressed during olive (*Olea europaea* L.) pollen ontog-eny. *BMC Plant Biol* **11:** 122.

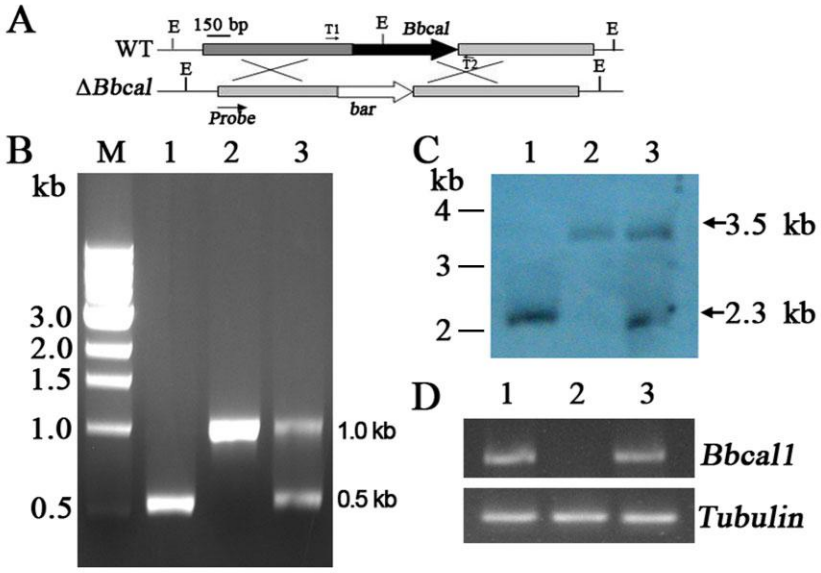

Fig. 1. Construction of mutant strains. A. Schematic diagram of vector, *Bbcal1* genomic locus and homologous recombination event. T1 and T2 indicated the positions of primers Pcal-t1 and Pcal-t2 respectively (Table S1). The position of the probe (150 bp) is given in the lower schematic, *bar* = phosphinothricin resistance marker, E = *Eco*RI restriction sites. B. PCR verification of correct integration event. PCR products using *Bbcal1* gene amplification primers and genomic DNA from; Lane 1, wild-type *B. bassiana*; lane 2, *Bbcal1*; lane 3, *Bbcal1:Bbcal1* complemented strain; and lane M, molecular size standards. C. Southern blot analysis of caleosin mutants. Genomic DNA was digested with *Eco*RI and probed with *Bbcal1* ORF gene fragment. Lane 1, wild-type *B. bassiana*; lane 2, *Bbcal1*; lane 3, *Bbcal1:Bcal1* complemented strain. The electrophoretic positions and sizes of the DNA bands are indicated. D. RT-PCR analysis of *Bbcal1* (top panel) and tubulin (bottom panel) expression. Lane 1, wild-type *B. bassiana*; lane 2, *Bbcal1*; lane 3, *Bbcal1* complemented strain.

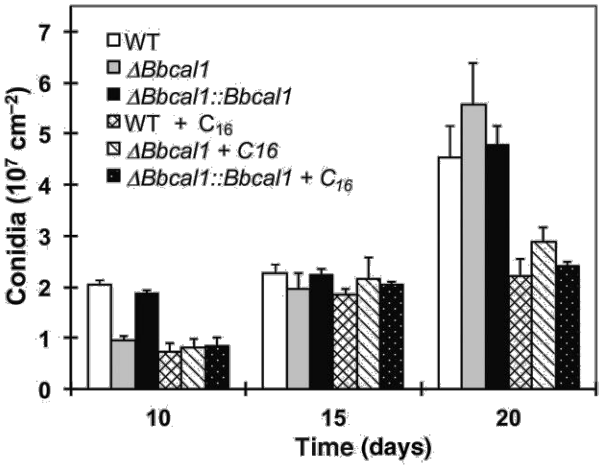

Fig. 2. Time-course of conidial yield of wild-type, *Bbcal1* and *Bbcal1::Bbcal1* strains grown on PDA and PDA supplemented with C16. Error bars: ± SD.

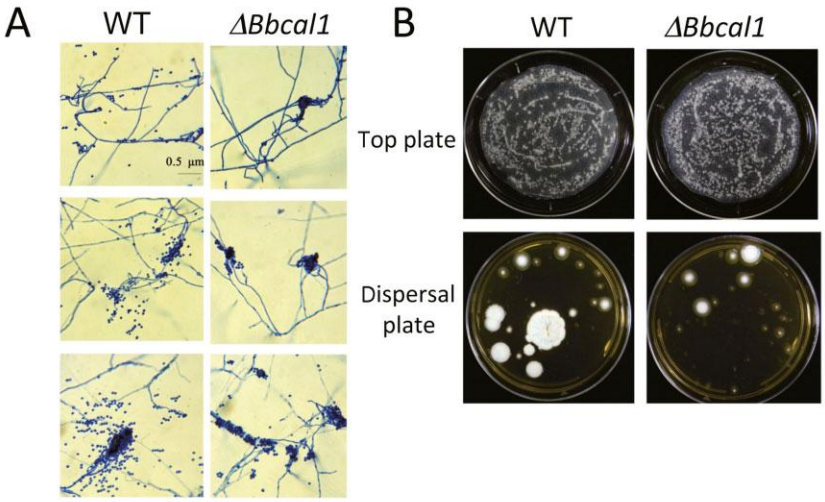

Fig. 3. Spore phenotypes of wild-type and *Bbcal1* strains. A. Differential interference contrast images of conidial formation after 9 (top panels), 12 (middle panels) and 15 (lower panels) days. B. Example of spore dispersal plates. Petri dishes were poured with growth media on both the top and bottom wells of the plates. Fungal strains were then inoculated on one side (top plate) and allowed to grow for 12–15 days. The number and distribution of spores 'dispersing' to the bottom 'dispersal' plate were then quantified.

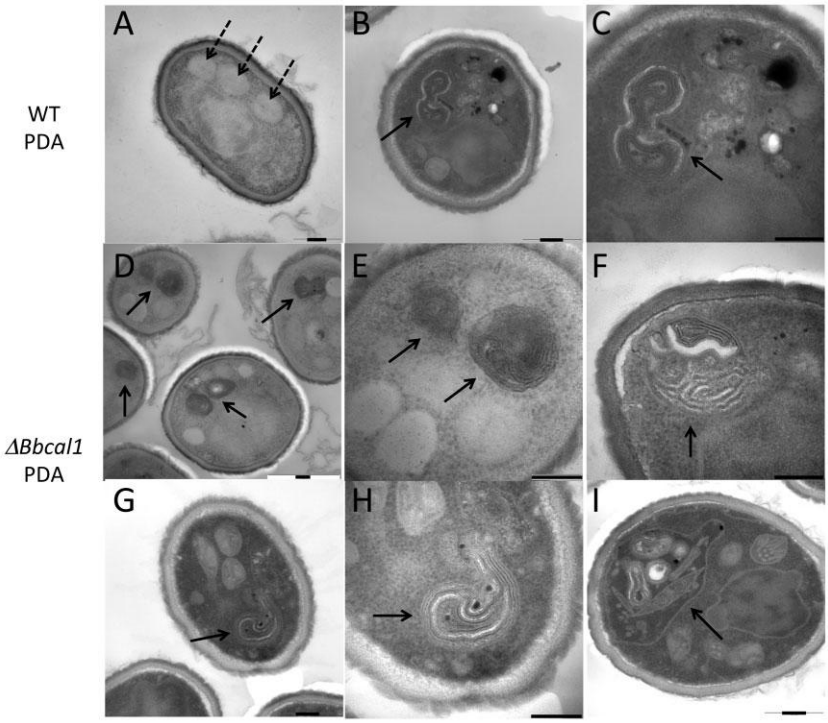

Fig. 4. Representative transmission electron micrographs of wild-type and *Bbcal1* conidia harvested from PDA. Conidia were grown, harvested and analysed as described in the Experimental procedures section. Dashed arrows indicate lipid bodies and regular arrows indicate multilamellar structures or other deformities. All scale bars = 200 nm.

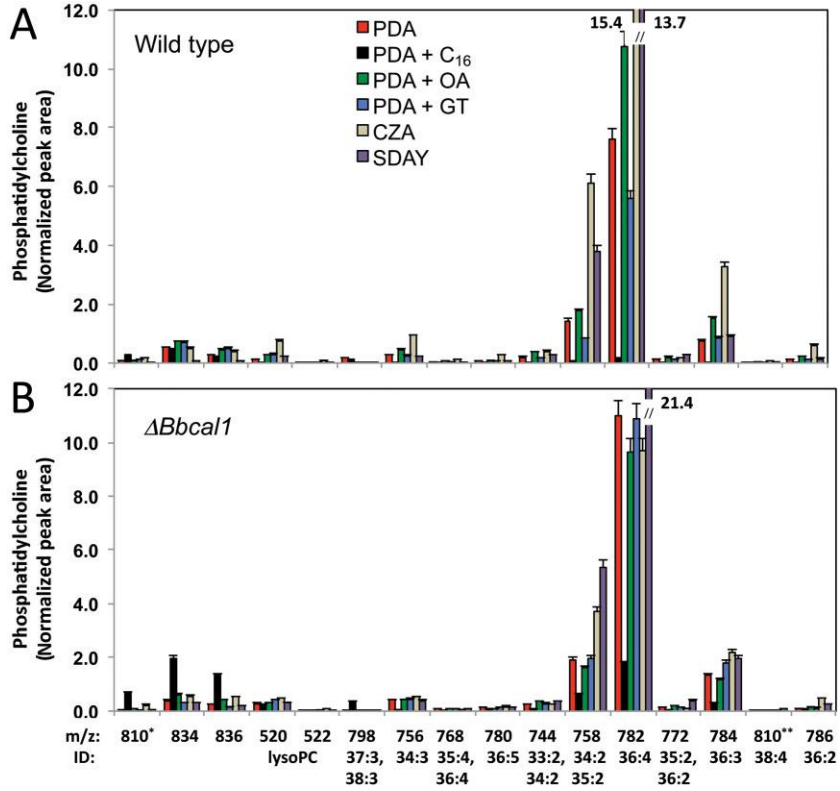

Fig. 6. Phosphatidylcholine analysis of wild-type (top panel) and *Bbcal1* (bottom panel) conidia grown on various media as indicated including PDA (red), PDA + C16 (black), PDA + oleic acid (OA, green), PDA + glyceride trioleate (GT, blue), CZA (grey) and SDAY (purple). Conidia were grown, harvested and analyzed as described in the Experimental procedures section. Error bars: ± SD.

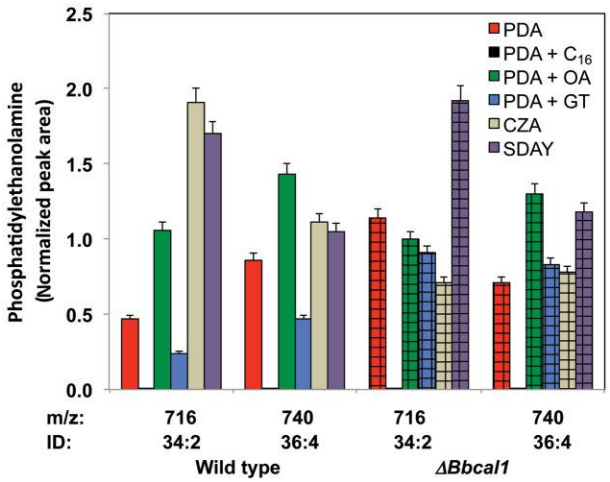

Fig. 7. Phosphatidylethanolamine analysis of wild-type and *Bbcal1* conidia grown on PDA (red), PDA + C16 (black), PDA + oleic acid (OA, green), PDA + glyceride trioleate (GT, blue), CZA (grey) and SDAY (purple). Conidia were grown, harvested and analyzed as described in the Experimental procedures section. Error bars: ± SD.

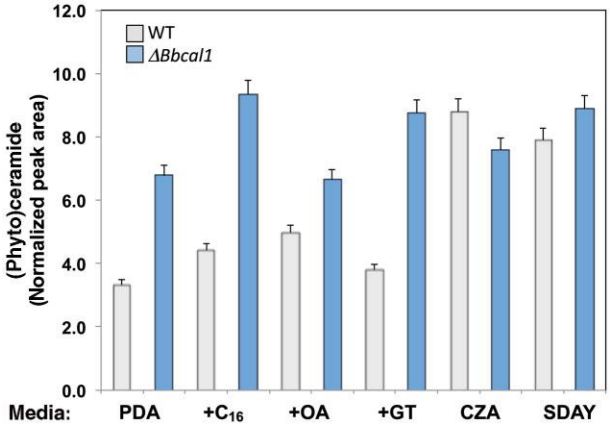

Fig. 8. Phytoceramide analysis of wild-type (grey) and *Bbcal1* (blue) conidia harvested from PDA, PDA + C16, PDA + oleic acid (OA), PDA + glyceride trioleate (GT), CZA and SDAY. Conidia were grown, harvested and analyzed as described in the Experimental procedures section. Error bars: ± SD.

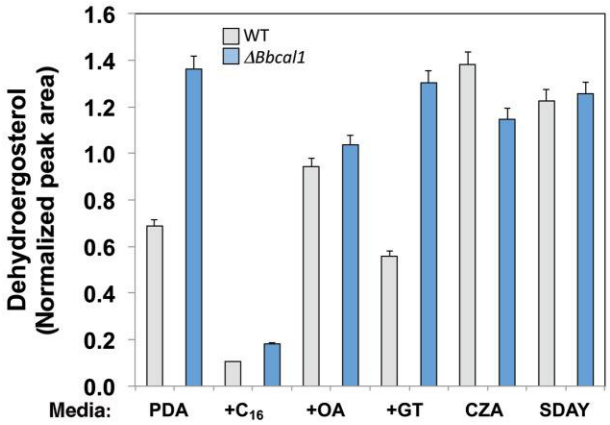

Fig. 9. Dehydroergosterol analysis of wild-type (grey) and *Bbcal1* (blue) conidia harvested from PDA, PDA + C16, PDA + oleic acid (OA), PDA + glyceride trioleate (GT), CZA and SDAY. Conidia were grown, harvested and analyzed as described in the Experimental procedures section. Error bars: ± SD.

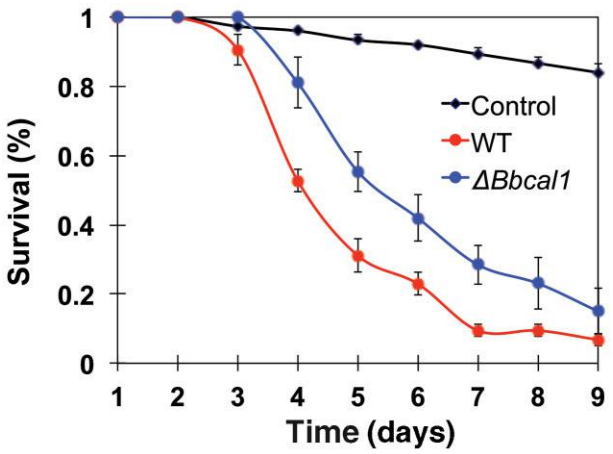

Fig. 10. Insect bioassays. *G. mellonella* larvae were treated with conidia from wild-type *B. bassiana* (red circles), *Bbcal1* (blue circles) or mock-treated controls (black triangles), as described in the Experimental procedures section. The percentage mortality over the indicated time-course is presented. Error bars: ± SD.

Supporting information

Additional Supporting Information may be found in the online version of this article at the publisher's web-site:

Fig. S1. Domain structure and alignment of *Bbca11* and related proteins obtained using CLUSTAL X. (A) Schematic diagram of caleosin inserted into the lipid monolayer. The cytoplasmic N-terminal domain contains an EF Ca^{2+} binding motif, followed by an anti-parallel hydrophobic stretch, con-taining a two-proline loop or 'knot'. (B) Amino acid alignment of Bbcal1 (XP008600624.1) with most highly similar sequences; Cmcal1, *Cordycepsmilitaris* (XP0066734971), Mocal1, *Magnaporthe oryzae* (XP003717404) and Cgcal1, *Colletotrichum graminicola* (EFQ36012.1), as well as the plant caleosins Atcal1, *Arabidopsis thaliana* (AEE85247.1) and Oscal1, *Oryza sativa* (EEC77624.1). The EF Ca^{2+} motif (red), hydrophobic stretches (yellow) and proline knot (blue) motifs are indicated. Conserved prolines in the fungal sequences are boxed. The proline knot sequences in the plant caleosins are underlined.

Environmental Microbiology, **17**, 4600–4614

Fig. S2. Response of *B. bassiana* *Bbcal* mutant to various stress conditions. Growth of *B. bassiana* wild type and *Bbcal1* strains in CZA plate supplemented with 2 mM EGTA (+0.01% bromocresol purple), PDA plates with either 1.5 M KCl, 1.5 M sorbitol or 100 μg ml^{-1} Congo red after inoculation of 1 μl of 5×10^6 spores ml^{-1} in the plate and incubation at 26°C for 7–10 days.

Fig. S3. Nile red staining of *B. bassiana* wild type and *Bbcal1* cells. Conidia and germinated conidia grown in PDB for 14 h or on locust hinder wings for 24 h were stained with Nile red as described in the Experimental procedures section.

Table S1. Primers used in this study.

Supplemental Table S1. Primers used in this study.

Name	Sequence (5' to 3')	Use
PcaL1	CCCAAGCTTCCTGTTCGAGCACTGGAAGA	KO strain construction
PcaL2	CAATATCATCTTCTGTCGACGTTCCAAGATTGA CTGAGGA	"
PcaR1	GCCCGTCACCGAGATCTGAAAGTTGGCACTCCA CTGACC	"
PcaR2	GCTCTAGAATGCAAGCCGTGTTGAATGC	"
pBar1	GTCGACAGAAGATGATATTGA	
pBar2	TCAGATCTCGGTGACGGGC	
Pcal-t1	ACGCGTTATTCGGACCGCTC	KO screening
Pcal-t2	GTTGCAACACCGGTCAGTGG	"
Pcal1	GGACTAGTCTTGCTACGAACTGCTCCTA	Complementation vector
Pcal2	TCCTCGCCCTTGCTCACCATTGAGCGAGACGCC CTTTGGC	"
Pcal-S	GGGTCCTAATTTCGCCGCAA	Southern blot
Pcal-rt1	TACTCGACTGACAAGGAGAG	Q-RT PCR
Pcal-rt2	GCTTTGCGGCAATGTGGTAG	"
Pactin-1	GTCAAGTCATCACCATTGGC	*Bbactin* RT-PCR
Pactin-2	GAGGAGCAATGATCTTGACC	
Pgpd-1	TCGACCTGACTGCTCGTCTT	*Bbgpd* RT-PCR
Pgpd-2	TAGGAGATAAGGTCCAGGA	
Ptub-1	TACTCTACGATTCGTCAAGT	Bbtubulin RT-PCR
Ptub-2	TGCTGGAACAGAGCCGTCTT	

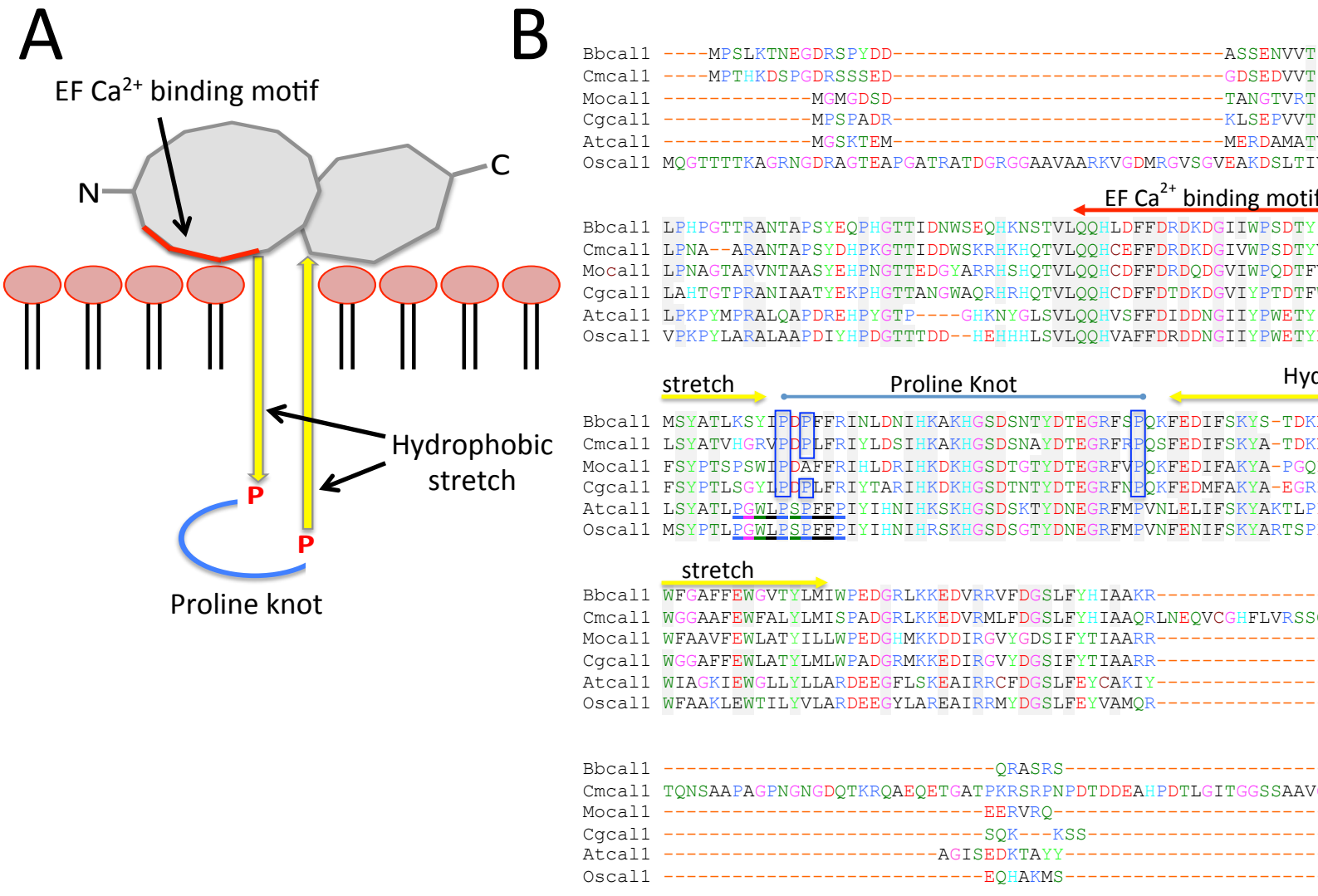
A
EF Ca2+ binding motif
N
C
Hydrophobic stretch
P
P
Proline knot
B
Bbcal1 ----MPSLKTNEGDRSPYDD----------ASSENVVT
Cmcal1 ----MPTHKDSPGDRSSSED----------GDSEDVVT
Mocal1 ----------MGMGDSD----------TANGTVRT
Cgcal1 ----------MPSPADR----------KLSEPVVT
Atcal1 ----------MGSKTEM----------MERDAMAT
Oscal1 MQGTTTTKAGRNGDRAGTEAPGATRATDGRGGAAVAARKVGDMRGVSGVEAKDSLTI
EF Ca2+ binding motif
Bbcal1 LPHPGTTRANTAPSYEQPHGTTIDNWSEQHKNSTVLQQHLDFFDRDKDGIIWPSDTY
Cmcal1 LPNA--ARANTAPSYDHPKGTTIDDWSKRHKHQTVLQQHCEFFDRDKDGIVWPSDTY
Mocal1 LPNAGTARVNTAASYEHPNGTTEDGYARRHSHQTVLQQHCDFFDRDQDGVIWPQDTF
Cgcal1 LAHTGTPRANIAATYEKPHGTTANGWAQRHRHQTVLQQHCDFFDTDKDGVIYPTDTF
Atcal1 LPKPYMPRALQAPDREHPYGTP----GHKNYGLSVLQQHVSFFDIDDNGIIYPWETY
Oscal1 VPKPYLARALAAPDIYHPDGTTTDD--HEHHHLSVLQQHVAFFDRDDNGIIYPWETY
stretch
Proline Knot
Hyd
Bbcal1 MSYATLKSYIPDPFFRINLDNIHKAKHGSDSNTYDTEGRFSPQKFEDIFSKYS-TDK
Cmcal1 LSYATVHGRVPDPLFRIYLDSIHKAKHGSDSNAYDTEGRFRPQSFEDIFSKYA-TDK
Mocal1 FSYPTSPSWIPDAFFRIHLDRIHKDKHGSDTGTYDTEGRFVPQKFEDIFAKYA-PGQ
Cgcal1 FSYPTLSGYLPDPLFRIYTARIHKDKHGSDTNTYDTEGRFNPQKFEDMFAKYA-EGR
Atcal1 LSYATLPGWLPSPFFPIYIHNIHKSKHGSDSKTYDNEGRFMPVNLELIFSKYAKTLP
Oscal1 MSYPTLPGWLPSPFFPIYIHNIHRSKHGSDSGTYDNEGRFMPVNFENIFSKYARTSP
stretch
Bbcal1 WFGAFFEWGVTYLMIWPEDGRLKKEDVRRVFDGSLFYHIAAKR----------
Cmcal1 WGGAAFEWFALYLMISPADGRLKKEDVRMLFDGSLFYHIAAQRLNEQVCGHFLVRSS
Mocal1 WFAAVFEWLATYILLWPEDGHMKKDDIRGVYGDSIFYTIAARR----------
Cgcal1 WGGAFFEWLATYLMLWPADGRMKKEDIRGVYDGSIFYTIAARR----------
Atcal1 WIAGKIEWGLLYLLARDEEGFLSKEAIRRCFDGSLFEYCAKIY----------
Oscal1 WFAAKLEWTILYVLARDEEGYLAREAIRRMYDGSLFEYVAMQR----------
Bbcal1 ----------QRASRS----------
Cmcal1 TQNSAAPAGPNGNGDQTKRQAEQETGATPKRSRPNPDTDDEAHPDTLGITGGSSAAV
Mocal1 ----------EERVRQ----------
Cgcal1 ----------SQK---KSS----------
Atcal1 ----------AGISEDKTAYY----------
Oscal1 ----------EQHAKMS----------

CZA + 2 mM EGTA

PDA + 1.5 M KCl

PDA + 0.5 M $CaCl_2$

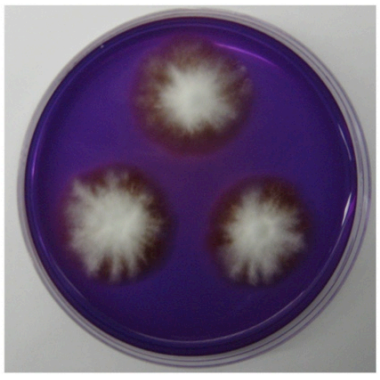

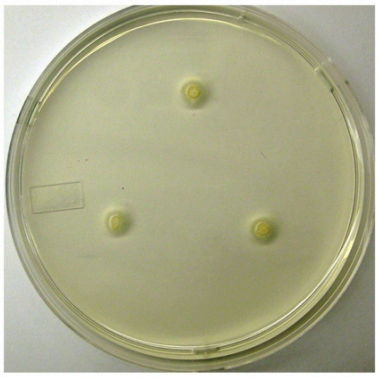

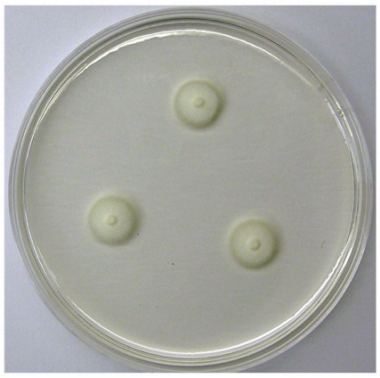

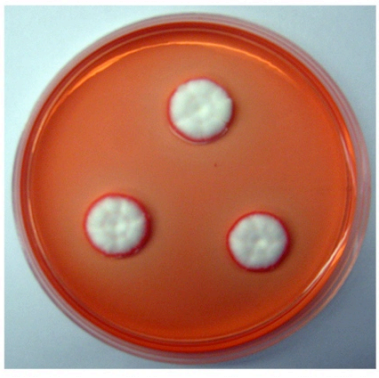

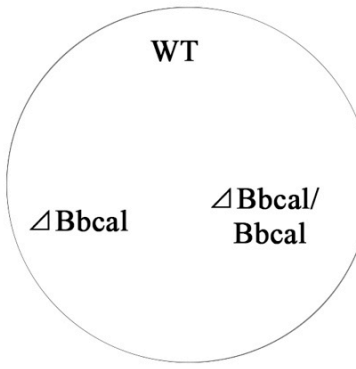

PDA + 1.5 M sorbitol

PDA + 25 mg/ml CGR

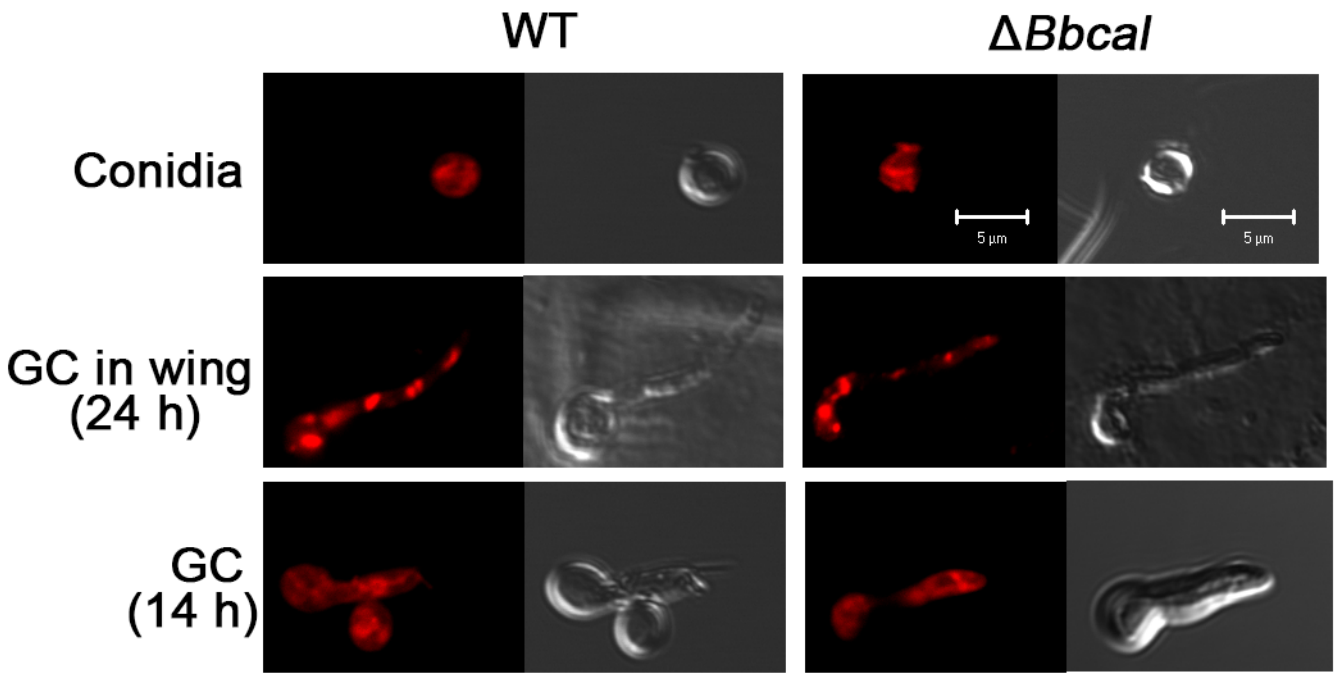
WT
ΔBbcal
Conidia
GC in wing
(24 h)
GC
(14 h)
5 µm
5 µm